frontiers | Frontiers in Earth Science

TYPE Original Research
PUBLISHED 21 December 2023
DOI 10.3389/feart.2023.1184671

OPEN ACCESS

EDITED BY
Stergios D. Zarkogiannis,
University of Oxford, United Kingdom

REVIEWED BY
Constance Choquel,
Lund University, Sweden
Georg Schulz,
University of Basel, Switzerland
Shunichi Kinoshita,
National Museum of Nature and Science, Japan

*CORRESPONDENCE
Katsunori Kimoto,
kimopy@jamstec.go.jp

RECEIVED 12 March 2023
ACCEPTED 22 November 2023
PUBLISHED 21 December 2023

CITATION
Kimoto K, Horiuchi R, Sasaki O and Iwashita T (2023), Precise bulk density measurement of planktonic foraminiferal test by X-ray microcomputed tomography.
Front. Earth Sci. 11:1184671.
doi: 10.3389/feart.2023.1184671

Precise bulk density measurement of planktonic foraminiferal test by X-ray microcomputed tomography

Katsunori Kimoto[1]*, Rika Horiuchi[1], Osamu Sasaki[2] and Tomohiro Iwashita[3]

[1]Japan Agency for Marine-Earth Science and Technology (JAMSTEC), Yokosuka, Japan, [2]Tohoku University Museum, Sendai, Japan, [3]White Rabbit, Corp., Tokyo, Japan

X-ray Microcomputed Tomography (μCT) is rapidly becoming an important analytical technique for examining the precise morphometry of small objects. The most notable feature of this technique is that it enables nondestructive, highly accurate morphometric measurements at micrometer-order resolution. In the Earth sciences, this makes μCT extremely useful for clarifying how genetic associations and the surrounding environment affect the morphology of micro-sized organisms. However, the actual analytical methods and the points that must be considered to produce reliable data have rarely been discussed in detail. Here, to address this lack of discussion, we describe in detail our methodology for precise μCT-based morphometry by using a test of the planktonic foraminifer and marine calcifier *Globorotalia inflata*. In addition to demonstrating the long-term stability of our μCT setup and analytical approach, we also propose a new methodology for test bulk density calibration using artificial carbonate phantoms. We expect that μCT together with our artificial phantom-based methodology will be useful for calculating accurate test bulk densities of micro-sized marine calcifiers.

KEYWORDS

X-ray microcomputed tomography (μCT), CT number, planktonic foraminifera, test bulk density, artificial calcite phantoms

1 Introduction

μCT is a CT technique that allows precise morphological analysis of microfossils and other geological materials. This technique offers a notable advantage in the study of microfossils by allowing the simultaneous, nondestructive examination of their morphologies at both the outer surface and the internal structure, all on micrometer scales. Furthermore, this technique also allows for the quantification of morphological information, facilitating comparisons between different specimens or cryptic species and more accurate identification of species compared with stereomicroscope and scanning electron microscope (SEM) techniques (e.g., Briguglio et al., 2014; Ikenoue et al., 2016; Shimizu et al., 2017; Xiao et al., 2017; Kachovich et al., 2019).

Planktonic foraminiferal tests have traditionally been used as a tool to reconstruct past and present marine environmental conditions. Many planktonic foraminifera develop a secondary crust layer as they reproduce, covering the thinner primary layer they formed at the end of growth (Brummer et al., 1987; Erez, 2003). This secondary calcification is

primarily a mature characteristic and is formed in deeper water during growth (e.g., Arikawa, 1983; Lohmann, 1995). The theoretical model of Lohmann (1995), which addresses the effects of secondary layer formation and selective dissolution of the primary layer on the isotope composition of the test, subsequently led to the development of two new proxies of carbonate chemistry of seawater in the past ocean (e.g., Broecker and Clark, 2001); Size-normalized shell weight (SNW; e.g., Barker and Elderfield, 2002; Bijma et al., 2002; Moy et al., 2009; Beer et al., 2010; Aldridge et al., 2012; Naik et al., 2013) and area-normalized shell weight (ANW; e.g., Marshall et al., 2013; Osborne et al., 2016; Weinkauf et al., 2020) are representative proxies of $[CO_3^{2-}]$ of sea water. These proxies are obtained by normalizing the test weight (mass) by the test length or test area determined from a SEM image of the test. However, such images are two-dimensional projection images, which makes it difficult to assess the accuracy of these proxies. Because the test of planktonic foraminifera has a curvature shape and its walls consist of a dense and complex structure composed of multiple layers with organic matter and calcium carbonate (Schiebel and Hemleben, 2017). Thus, SNW and ANW are indirect measurements of test density.

Three-dimensional morphometry with μCT has the potential to solve the above problems. The application of μCT for estimating the carbonate solubility and calcification capacity of marine calcareous materials has recently been widely discussed (Johnstone et al., 2010; Iwasaki et al., 2015; 2019a; Todd et al., 2020; Zarkogiannis et al., 2020; Kinoshita et al., 2021; Kuroyanagi et al., 2021; Ofstad et al., 2021; Charrieau et al., 2022). Furthermore, ambitious attempts have been made to estimate the concentration of carbonate ions in past seawater by quantifying the dissolution of foraminifera tests (e.g., Iwasaki et al., 2019b; 2022), habitat depth (Zarkogiannis et al., 2022), and to detect the biological effects of anthropogenic environmental changes since the Industrial Revolution (Fox et al., 2020).

To date, the methodology, accuracy, and reproducibility of densitometry of microfossil using μCT are yet to be discussed in detail. Here, we set out to describe in detail the collection of measurements by μCT analysis and precautions that must be considered. In addition, we also discuss the stability of μCT measurements for the analysis of foraminiferal tests, as well as the development and application of new reference materials for density measurement of calcium carbonate.

2 Methodology

2.1 Samples

The target specimen was a single test of the planktonic foraminifer *Globorotalia inflata* that was recovered from water pumped from the surface of the Kuroshio Current in the western North Pacific. The reference material for μCT measurement was a single grain of limestone crystal formed from stable oxygen and carbon isotopes (NBS19, NIST RM8544) (Iwasaki et al., 2015). The grains of this material are uniform in density, are readily available, and are used as a reference material in Earth-science laboratories around the world (currently unavailable, but extant in labs around the world). The reference material was analyzed at the same time as the target specimen, which allowed for later adjustments to be made to offset energy fluctuations in the X-ray radiation produced from the X-ray tube. To prepare the standard material, the limestone grain was gently dissolved in a weak acid (0.01 M HCl), molded with a brush into a spherical-to-subspherical shape, and used as a standard sample to average the X-ray transmission distance.

In μCT analyses, objects exposed to X-ray irradiation generate heat on their surface, which may cause the adhesive used to fix the object to the rotation stage to melt and the sample to become loose and move during analysis. For this reason, the exposure time should be set as short as possible, and complete fixation of the object is important. Tragacanth and other similar adhesives that are commonly used for fixing microfossils easily become flexible under heat; therefore, here we used a urethane adhesive with much better heat resistance (Jellafin; SEC Seaprex, Co., Ltd., Hakodate, Japan).

2.2 X-ray irradiation

The principal equipment and analytical parameters used in this study are shown in Table 1. In this study, the tube voltage and current were set at 80 kV and 50 μA, respectively, and the target current was 10.5 μA. Multiple stacking (averaging multiple images acquired at the same projective position) is an effective way to increase the signal-to-noise ratio when acquiring transmission images; in particular, the effect of noise generated by the air around objects can be markedly reduced. In consideration of the balance between image acquisition time and improvement of the signal-to-noise ratio, four images were averaged to obtain a single image. The projection number was set at 1,200 for an X-ray detector size of 992 × 992 pixels (1 × 1 binning).

2.3 Beam hardening

When an object is irradiated with white X-rays with a wide energy distribution, the X-rays with high energy preferentially penetrate through the object, whereas those with low energy are absorbed at the outer surface of the object or by surfaces inside the material and reach the detector only after attenuation. This selective absorption of X-rays is called beam hardening (BH), and it often adversely affect for density measurements of microfossils made using μCT (Briguglio et al., 2014). To reduce the intensity of BH artifacts, a metal filter can be inserted in front of the X-ray source. In a simulation examining the transmitted X-ray energy distribution obtained with various metal filters at an X-ray tube voltage of 80 kV, the greatest suppression of X-ray transmission in the low-energy region less than 20 kV, which is the primary cause of BH, was obtained with 200-μm-thick, high-grade aluminum (>99.0% Al). In the present study, we therefore used a 200-μm-thick Al filter in front of the X-ray detector (Ay et al., 2012). This filter was used for all of the test bulk density measurements.

To evaluate the effect of BH, it is useful to monitor the gray values of the reconstructed image of a homogeneous reference material (phantom) made of the same material as the target and measured at the same time as the target. If BH artifacts do not appear in the cross-section of the reference material at a similar transmission distance to the target specimen, it is safe to assume that the BH effect is weak in the target specimen. Conversely, if BH does appear in the cross-section, we

TABLE 1 Principal equipment and analytical parameters used in the study.

X-ray tube	L10711-03 (hamamatsu photonics)
X-ray detector	PaxScan 1313DX (1024x1024 pixels, Varex Imaging)
Tube Voltage (kV)	80
Tube current (μA)	50
Target current (μA)	10.5
X-ray focal point size (μm)	0.8
Cumlative number of images	2
Number of image acquisition/sec	3
Projection number	1,200
Resolution (μm)/pixel	1.00
Binning	1 x 1 (992x992)

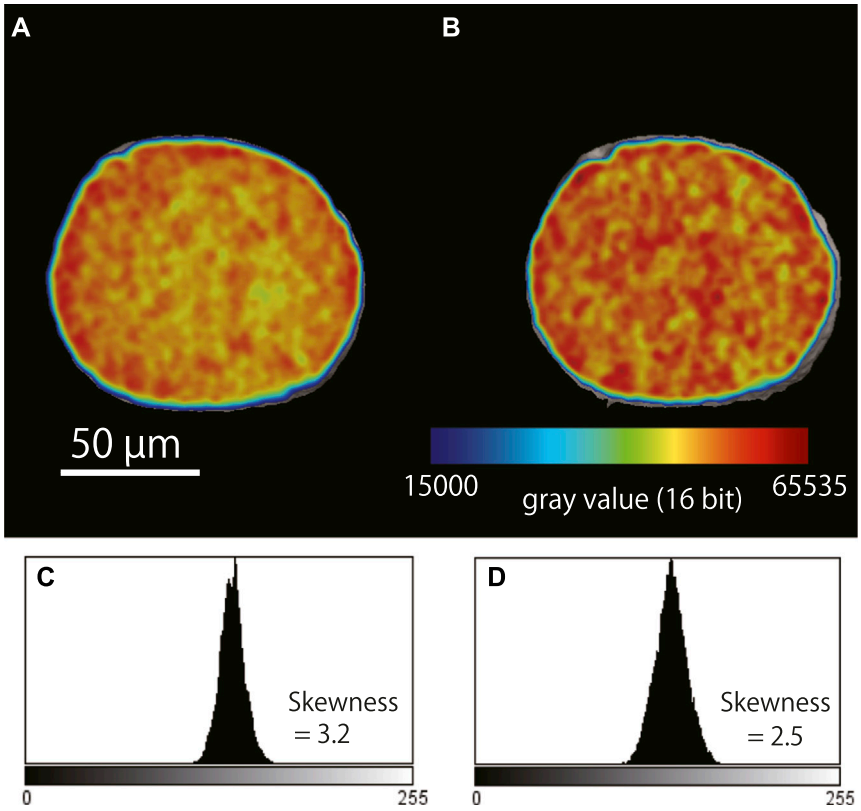

FIGURE 1
Examples of beam hardening artifacts in a cross-section of the limestone reference material (NBS19) before and after correction. **(A)** Cross-section image of the reference material obtained without a metal filter. High gray values (red) are seen around the edge of the reference material, and lower values (yellow) are seen at the center. **(B)** Cross-section image of the same reference material obtained with a 0.2-mm thick aluminum filter placed in front of the X-ray detector; the gray values are overall more homogeneous compared with what was observed without the filter. **(C)** Frequency distribution of the gray values in **(A)**. **(D)** Frequency distribution of the gray values in **(B)**.

should assume that the target specimen at transmission distances greater than the diameter of the reference material are affected by BH. In the present study, the diameter of the limestone reference material was selected to match the total length of the X-ray transmission distance through the foraminiferal tests; the presence or absence of BH artifacts was evaluated by examining the gray values of a cross-section image of the limestone. Thus, a limestone grain with a diameter of 100–300 μm was used, and the difference of the gray value between approximately 100 pixels at the outer edges or in the center was within 2% on average and was reduced to 10%–20% of that obtained without

the metal filter (Figure 1). Thus, in this study, BH up to a calcium carbonate thickness of 100–300 μm was considered to be corrected by the aluminum filter. In practice, the total X-ray transmission length of planktonic foraminiferal walls is less than 300 μm, and many species have high porosity due to the presence of pores in the wall. Therefore, the above method should be applicable for test bulk density analysis of almost all planktonic foraminiferal tests.

In this study, a grain of limestone (NBS 19; ~130 μm in diameter; 2.71 g/cm^3 in true density; 1,000 in mean CT number) was used to normalize the CT number of foraminiferal tests. (Iwasaki et al., 2019a).

2.4 CT number as an index of the relative density of calcium carbonate

In analyses of human bone density, the following CT numbers are often used: −1,000 (air), 0 (water), and 1,000 (highest bone density) (Hounsfield, 1980). CT number is calculated in Hounsfield units (HU; named after the proponent of this number) by using the following equation:

$$\text{CT number} = \frac{\mu(\text{tissue}) - \mu(\text{water})}{\mu(\text{water}) - \mu(\text{air})} \times 1000, \quad (1)$$

where μ is the attenuation coefficient for each material.

The same concept can be applied to the calculation of the test bulk density of a foraminiferal sample. Although the attenuation coefficient and the gray value are not exactly the same physical quantity, they are both parameters related to the attenuation of X-rays, and the relative relationship holds. Therefore, they can be made dimensionless and expressed as a relative density by normalizing by the gray value of the standard sample (Iwasaki et al., 2015).

The relative number of gray values between the sample and standard material is called the calcite CT number (hereafter simply CT number), defined by the following equation:

$$\text{CT number} = \frac{\mu(\text{foram}) - \mu(\text{air})}{\mu(\text{standard}) - \mu(\text{air})} \times 1000, \quad (2)$$

where μ(foram), μ(air), and μ(standard) are the gray values of the foraminiferal test, the surrounding air, and the standard material, respectively. In the present study, the values of μ(air) and μ(standard) were set to 0 and 1,000, respectively. CT number refers to the value related to density only when the sample is composed of a homogeneous material and when the effect of BH is eliminated. In the case of foraminiferal tests composed of a single material, the bulk density of the test can be calculated from the CT number.

3 Calibration of accurate test bulk density: external calibration with artificial phantoms

In X-ray CT scanning, a reference sample (e.g., air or water) and a target sample are scanned simultaneously, and the CT numbers of the tomographic image (e.g., Hounsfield scale of medical CT) are calibrated from the grayscale of the image based on the gray values of the reference sample. The development of a suitable CT number calibration method is the most important issue in the application of μCT. There are currently no commercially available reference materials (phantoms) that mimic the bulk density of small grains of calcium carbonate such as the foraminiferal tests. To maintain the external accuracy of the measured bulk density, independent comparative calibration phantoms are needed. Therefore, we produced our own calibration phantoms as follows.

1) Pure artificial calcium carbonate powder (~5 μm particle diameter; >99.9% purified, chemical analysis grade) was used to make the phantoms. Calcium carbonate powder was placed in a die set and exposed to pressures from 1.5 to 10 tons for 20 min to solidify the carbonate powder. These solidified calcium carbonate samples were named “die samples”.
2) The die samples were gently removed from the die set and weighed to three decimal places in milligrams on a microbalance (Sartorius ME5; Sartorius Lab Inst. GmbH and Co., Germany). Then, the volume of the die samples was measured by μCT.
3) The test bulk density of the die samples was obtained by dividing the weight by the volume.
4) The die samples were molded into smaller pieces (<300 μm in diameter) by hand using a surgical knife under a binocular stereomicroscope and then used as the reference material in the foraminiferal test bulk density analysis.

This method yielded carbonate phantoms with various porosities (i.e., bulk densities) because different pressures result in different states of crimping between the calcium carbonate particles. To develop a calibration equation between test bulk density and CT number, we analyzed these phantoms and a single NBS19 grain by μCT under the same conditions as those used for the subsequent analysis of the foraminiferal test (Table 2).

To verify the stability of the CT number under the present experimental conditions, test bulk density analysis of a single foraminiferal test was repeated every 2 days for 2 months (Nov. To Dec. 2022). The reason for this period is that the tungsten filament in the X-ray tube runs out after about 2 months (ca. 300 h of operation) at the rate at which we operate our instrument; therefore, we needed to complete the experiment within 2 months so that all of the measurements were performed under the same conditions.

To evaluate the objectivity of this method for test bulk density, multiple weight measurements of single foraminifera were performed using electronic microbalances and the differences between the μCT and conventional methods were evaluated. A Cubis II MCA6.6S electronic microbalance (Sartorius Lab Instruments GmbH and Co., Germany) was used for the measurement of the single specimens. The measurements were performed at room temperature (25.7°C–26.0 °C) and humidity from 29% to 34%.

The μCT instrument used in this experiment was a ScanXmateDF160TSS105 (Comscantechno Co., Ltd., Yokohama, Japan) installed at the Japan Agency for Marine-Earth Science and Technology (JAMSTEC, Kanagawa, Japan). The same tungsten filaments and tungsten targets were used throughout the experiment. The same experimental settings were used for all the analyses. Reconstructions and drawings of images were obtained by using the coneCTexpress and Molcer Plus 3D image visualization

TABLE 2 Data of die samples and calibration phantoms used in this study.

Die samples				
#ID	Volume ($\times 10^3$ μm^3)	Weight (μg)	Weight STD	Remarks
P2	125.58	229.682*	0.007	*5 times average
P4	56.23	111.675*	0.004	*5 times average
P8	25.81	54.114*	0.012	*5 times average
Calibration phantoms				
ID	Volume ($\times 10^3$ μm^3)	CT number	CT number STD	Bulk density
P2-1	16.29	692.8	13.3	1.83
P4-1	9.45	745.4	10.3	1.99
P8-1	15.11	780.0	12.1	2.10
NBS19	0.32	1,000	-	2.71 (in theory)

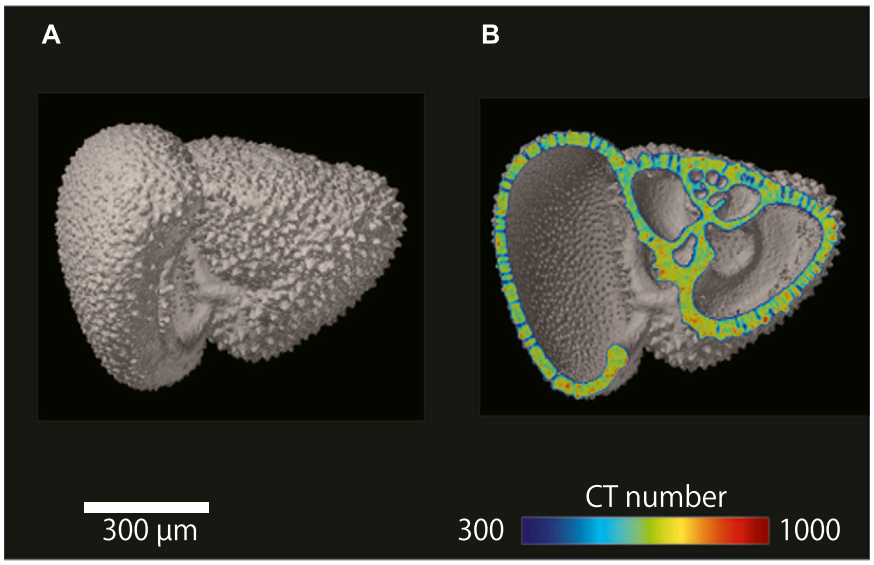

FIGURE 2
μCT images of a single shell of the planktonic foraminifer *Globorotalia inflata*. **(A)** Isosurface image of *G. inflata*. **(B)** Cross-sectional image of *G. inflata* with a color overlay showing CT number.

and processing software (White Rabbit, Corp., Tokyo, Japan), respectively. The general principle of Feldkamp cone-beam reconstruction was followed to reconstruct image cross-sections based on the filtered back-projection algorithm.

4 Results

4.1 Histogram and determination of the threshold of the 3D image

A single test of the planktonic foraminifer *G. inflata* was subjected to μCT to obtain isosurface and cross-sectional images (Figure 2). Segmentation is an important concept for making an isosurface image because it directly affects not only the quality of the reconstructed 3D image but also that of the subsequent analyses. Segmentation can be described as "thresholding" to distinguish regions of interest from other unwanted regions: areas higher than the threshold are displayed, whereas areas below it are ignored. Generally, 3D image processing software performs an automatic segmentation (e.g., by using Otsu's formula (Otsu, 1980)). However, in our method, since the threshold value changes with the shape of the histogram, the range of variation is large for low test bulk density samples with severe dissolution. To minimize measurement errors due to variations in threshold values, we clarified the relationship between the gray values of the air and

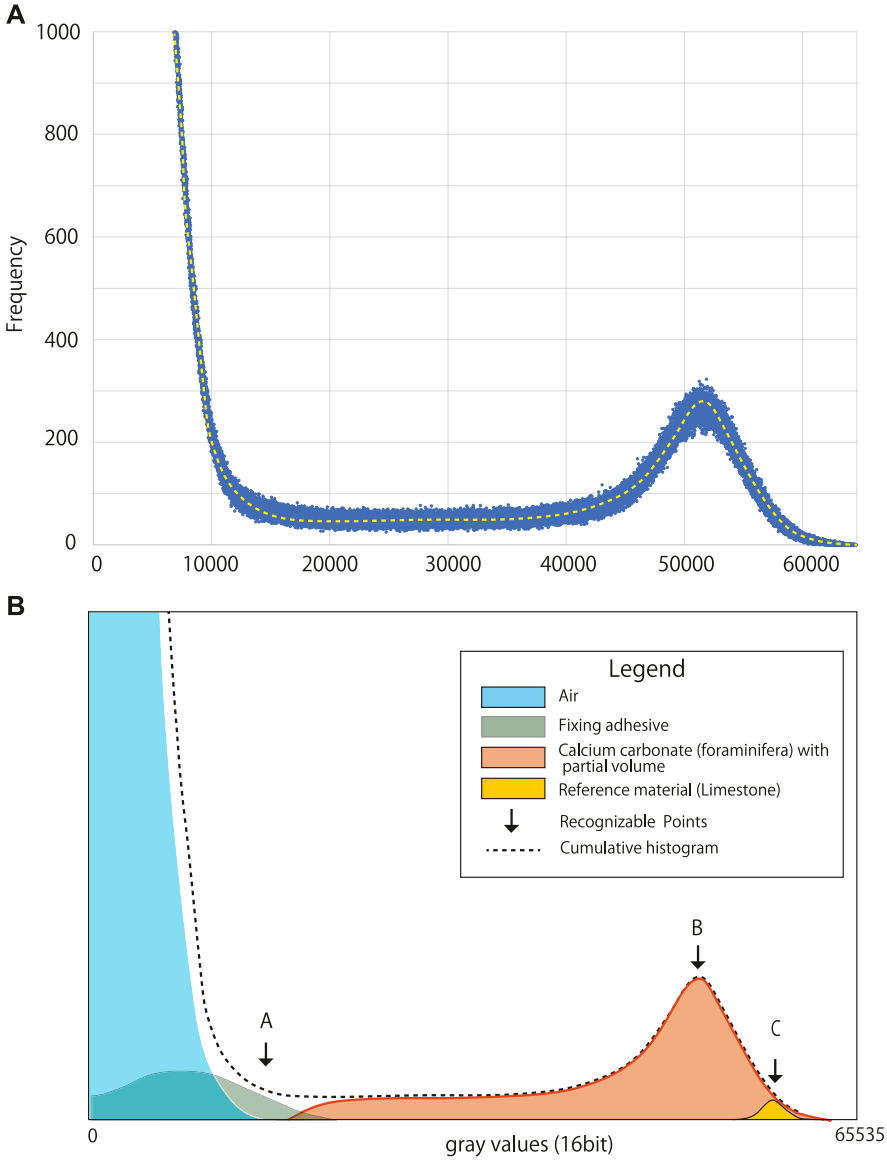

FIGURE 3
Histograms obtained for a 16-bit image of a single shell of the planktonic foraminifer *Globorotalia inflata*. **(A)** Original gray value histogram. **(B)** Diagram showing the peaks comprising the gray value histogram and recognizable control points. (A): maximum gray value of the air surrounding the specimen, (B): peak gray value for the foraminiferal shell, (C): peak gray value for the limestone reference material. The histogram was obtained by reconstructing each component separately after the μCT measurement.

the reference material, which are constantly visible during the measurement is in progress, and then calculated the threshold value.

Figure 3 shows the gray value histogram obtained for a 16-bit image of the foraminiferal test. The 16-bit image comprised grayscale voxels each with a value between 0 (lowest) and 65,535 (highest) (Figure 3A). The histogram contains four component peaks, one each for the air surrounding the foraminiferal test, the fixing adhesive, the foraminiferal test (calcium carbonate) including partial volumes, and the reference material (i.e., limestone) (Figure 3B). In the present study, the peak value of the air was set at a gray value of 0.

The peak attributed to the adhesive was almost fully contained within the peak for the air, which was expected because the adhesive used to fix the samples was purposely selected because of its low X-ray absorption, which greatly eases differentiation between the adhesive and the specimen during image processing.

A partial volume is defined as a voxel that contains both the specimen and the surrounding air. Therefore, the peak attributed to foraminiferal calcium carbonate represents a combination of the voxels only containing the foraminiferal test as well as the voxels containing partial volumes.

There was a marked difference in gray values between air and calcium carbonate because of the large difference in their densities,

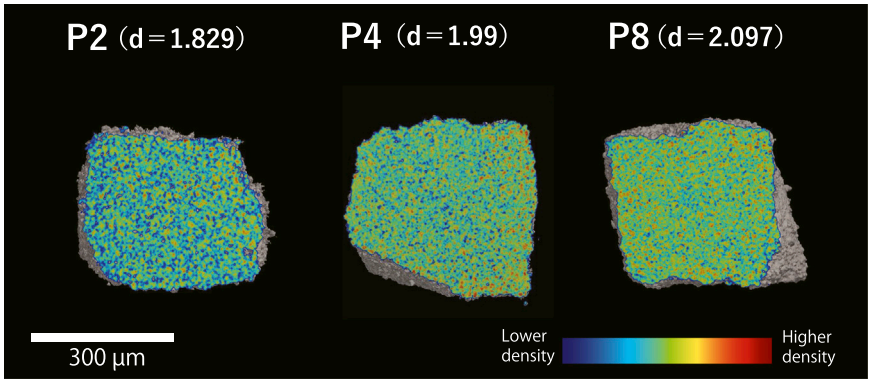

FIGURE 4
Cross-sectional images showing the density differences of the artificial calcite phantoms developed in the present study. Phantoms P2, P4, and P8 were each pressed for 10 min with weights of 2, 4, and 8 tons, respectively. Colors represent the relative density. D = bulk density.

which means they are well separated in the histogram of gray values (Figure 3B). The relative position between the upper gray value limit of air and the peak of the reference material depends on the sensitivity of the X-ray detector when the X-ray energy is constant; therefore, the relative location between the two should be constant under the same X-ray irradiation conditions. This relationship can be shown as a simplified ratio, response factor k, which indicates the relationship between the upper limit of air and the peak value of calcium carbonate (limestone) and can be calculated as follows:

$$k = \frac{\mu(\mathrm{CC})peak}{\mu(\mathrm{Air})max} \quad (3)$$

where μ(Air)max is the maximum gray value of the air and μ(CC) peak is the modal gray value of the reference material. Ideally, k should be constant, so if the peak position for the reference material can be identified, the lower boundary limit can be automatically determined. In the present study, all voxels with a value higher than the maximum gray value of air (i.e., the threshold value for binarization) were considered to contain calcium carbonate, and CT numbers were calculated.

The above concepts were used to investigate the long-term stability and reliability of the CT numbers obtained using the present μCT setup as well as to calculate the physical parameters related to test bulk density.

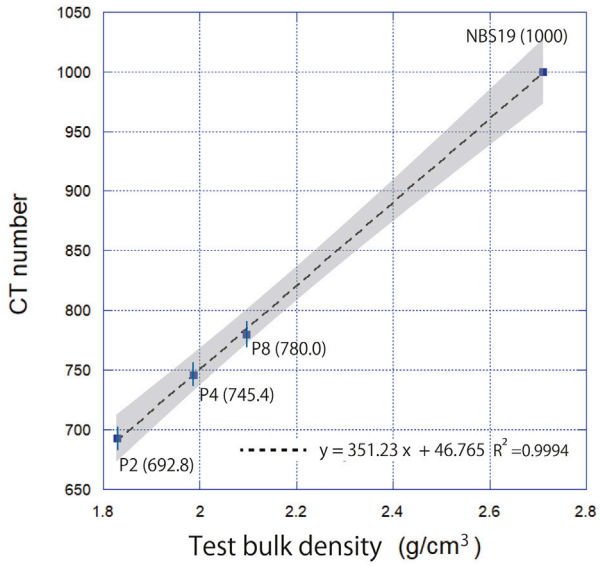

FIGURE 5
Relationship between test bulk density and CT number for the artificial carbonate phantoms (P2, P4, P8 with each CT number in parentheses) and reference material NBS19. The dotted line indicates the linear regression line (R^2 = 0.9994). The gray shading indicates the 95% confidence interval.

4.2 Calibration with our artificial carbonate phantoms

Based on the cross-sectional images (Figure 4), our artificial carbonate phantoms observed by μCT were considered to be sufficiently homogeneous for use as calibration phantoms. The relationship between the bulk density and CT number of the calibration phantoms is shown in Figure 5. For each calibration phantom, the CT number was measured 10 times, and the average value and relative standard deviation were calculated. The relationship between CT number and bulk density is described by the following linear regression equation:

$$\text{CT number} = 351.23 \times \text{test bulk density} + 46.765 \ (R^2 = 0.9994). \quad (4)$$

Thus, the response of the X-ray detector was proportional to the X-ray attenuation by the sample.

4.3 CT number and other physical properties of planktonic foraminifera

Over the 2-month investigation period, the CT number and other physical properties of a single foraminiferal test were

10.3389/feart.2023.1184671

TABLE 3 μCT analysis results and physical properties of *Globorotalia inflata* shells for the 2-month investigation period.

#Run	Air	NBS peak	*k*	CT number	Shell bulk denisty (g/cm^3)	Volume (×10^{6}μm^3)	Surface area (×10^{6}μm^2)	Average thickness (μm)	Calculated weight (μg)
1	15,421	49,234	3.2	853.7	2.30	9.3	1.344	13.9	21.4
2	15,400	48,822	3.2	863.4	2.32	9.4	1.348	14.0	21.9
3	14,192	48,314	3.4	851.5	2.29	9.6	1.359	14.2	22.0
4	14,602	48,859	3.4	856.7	2.30	9.5	1.334	14.2	21.8
5	15,953	49,507	3.1	854.5	2.30	9.3	1.323	14.1	21.5
6	14,862	48,218	3.2	867.1	2.33	9.5	1.339	14.1	22.1
7	15,011	48,909	3.3	849.5	2.28	9.4	1.353	13.8	21.4
8	14,581	49,992	3.4	853.5	2.30	9.4	1.344	14.0	21.6
9	15,687	49,298	3.1	853.1	2.29	9.5	1.337	14.3	21.9
10	14,602	48,000	3.3	865.0	2.33	9.5	1.355	14.0	22.0
11	14,786	49,589	3.4	845.0	2.27	9.5	1.313	14.4	21.5
12	14,540	49,858	3.4	851.6	2.29	9.5	1.332	14.2	21.7
13	13,915	49,568	3.6	839.6	2.26	9.6	1.335	14.3	21.6
14	14,458	48,447	3.4	857.6	2.31	9.4	1.352	13.9	21.7
15	13,690	48,544	3.6	850.3	2.29	9.6	1.341	14.3	21.9
16	13,147	48,610	3.7	842.8	2.26	9.7	1.318	14.8	22.1
17	12,461	48,424	3.9	847.9	2.28	9.8	1.345	14.5	22.3
18	11,714	48,642	4.2	845.7	2.27	9.8	1.410	13.9	22.3
19	12,779	49,048	3.8	850.2	2.29	9.8	1.355	14.4	22.3
20	14,233	48,418	3.4	865.9	2.33	9.4	1.360	13.9	22.0
21	14,520	48,482	3.3	853.8	2.30	9.5	1.339	14.2	21.8
22	14,356	48,920	3.4	847.5	2.28	9.5	1.351	14.1	21.6
23	14,049	42,499	3.0	856.9	2.30	9.4	1.398	13.4	21.6
24	14,888	48,249	3.2	853.9	2.30	9.3	1.328	14.0	21.3
25	13,905	48,249	3.5	854.3	2.30	9.6	1.359	14.1	22.1
26	14,735	48,644	3.3	858.5	2.31	9.4	1.352	13.9	21.7
27	14,509	47,443	3.3	869.9	2.34	9.5	1.327	14.3	22.2
28	15,564	47,744	3.1	853.5	2.30	9.5	1.360	14.0	21.8
29	15,851	50,039	3.2	857.3	2.31	9.3	1.357	13.8	21.5
30	15,759	49,771	3.2	862.0	2.32	9.3	1.351	13.8	21.6
31	16,516	48,000	2.9	871.0	2.35	9.4	1.346	13.9	22.0
Mean	14,538	48,592	3.4	854.9	2.30	9.5	1.347	14.08	21.8
STD	1,047.299	1,313	0.26	7.72	0.02	0.14	0.02	0.26	0.28
RSD%	7.2	2.7	7.8	0.9	1.0	1.5	1.5	1.9	1.3

examined a total of 31 times by μCT (Table 3). The mean upper gray value for the air was 14,538 (range, 14,538–16,516). The mean value of *k*, which indicates the responsiveness of the X-ray detector, was 3.4 (range, 2.91–4.15).

The average CT number was 854.9 (range, 839.6–871.0; standard deviation, 7.7; variability, 0.90%). The variability of CT number showed no clear trend over the 2-month investigation period (Figure 6).

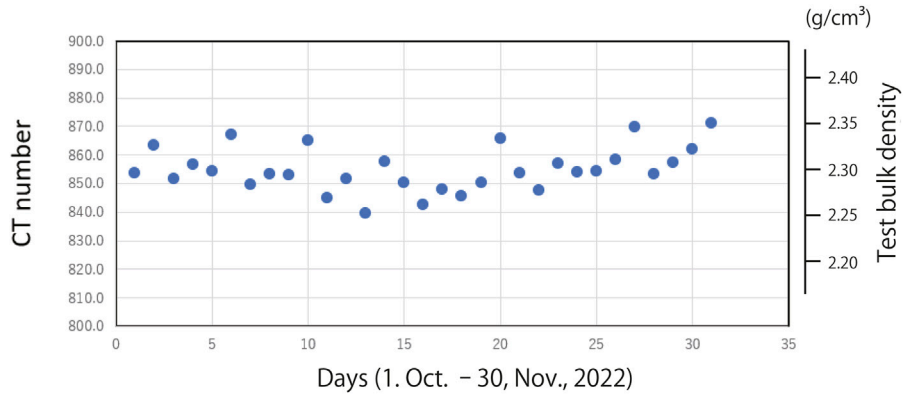

FIGURE 6
Distribution of CT number for the 31 analyses conducted over the 2-month investigation period.

TABLE 4 Average weight of a single *Globorotalia inflata* specimen measured 20 times using an electronic microbalance.

	Aluminum boat weight (mg)	*G. inflata* weight (mg)	Calculated shell bulk density (g/cm³)
Mean (20 measurements)	1.946	0.029	3.244
STDEV	0.002	0.002	0.266
RSD (%)	0.11	8.21	8.21
			Room temp: 25.7 °C
			Humidity: 29% (26.0 °C)

4.4 Stability of weight measured by electronic microbalance

Table 4 shows the weight of one individual test of *G. inflata* measured 20 times by using an electronic microbalance. The average weight was 0.029 mg and the standard deviation was 0.002 mg (8.21%). The weights of the individual tests fell within the range of already published values (9.65–59.59 μg; Haarmann et al., 2011). However, the calculated test bulk density was 3.24 g/cm³, which was slightly higher than the theoretical density of limestone (2.71 g/cm³). A possible reason for this discrepancy was that cytoplasm was still present in the test chamber, which was confirmed by examination of the transparent μCT image. It is difficult to estimate the weight of dried cytoplasm from a μCT image; however, assuming that the average test bulk density (2.30 g/cm³) calculated by μCT is correct, the weight of dried cytoplasm in a *G. inflata* test is estimated to be 0.0085 mg. The total chamber volume of the *G. inflata* examined in this experiment was calculated to be 0.015 mm³. Assuming that the density of the cytoplasm is almost equal to that of seawater, its weight is almost half the weight of the seawater that fills this volume. Thus, this experiment shows that using the weights of single individuals measured on an electronic microbalance does not provide accurate estimates of test bulk density due to the effect of the cytoplasm inside the foraminiferal test. Thus, the measurement of test bulk density by microbalance may not be appropriate for all contexts.

5 Discussion

5.1 Bulk density calibration by using artificial carbonate phantoms

Although artificial phantoms exist to calculate human bone density, measuring the bulk density of carbonate particles using an artificial phantom of pure calcium carbonate has never been investigated. In the present study, the relationship between artificial carbonate phantoms and CT number showed a clear relationship, indicating that there is a linear relationship between the bulk density of calcium carbonate particles and the responsiveness of the X-ray detector (Figure 5). Thus, our findings show that test bulk density measurement using artificial carbonate phantoms is feasible. Furthermore, this approach identifies and eliminates impurities present in the foraminiferal test from the image, allowing only the volume of the test to be measured. This provides a new methodology for obtaining accurate test weights for samples that may contain sediment or cytoplasm.

Based on above methodology, test bulk density was calculated. Using Eq. 4, the mean test bulk density and weight of single test of *G. inflata* calculated from the CT number was 2.3 ± 0.02 g/cm³ and 21.8 ± 0.28 μg, respectively. This value was close to the average bulk density reported for several species of planktonic foraminifera in the western North Pacific (Iwasaki et al., 2019a) and was within the weight range reported for individual *G. inflata* in modern water (Haarmann et al., 2011).

The average volume and surface area of the foraminiferal test calculated from the isosurface image was 9.5×10^6 μm^3 and 1.347×10^6 μm^2, respectively; variability was 1.5% for both. The average thickness, calculated by dividing the volume of the foraminieral test by one-half the surface was 14.1 μm, with a variability of 1.9%. No long-term trends over the 2-month investigation period were observed for the three observed parameters.

5.2 Long-term stability and reliability of CT number and other parameters

The CT number determined for the foraminiferal test was very stable over the 2-month investigation period (Figure 6). Variability remained within 0.9%, and no systematic fluctuations were observed. The volume and surface area also had a high reproducibility of 1.5% each. The calculated weight averaged 21.8 μg with an STD of 0.28 μg. This variability is comparable to and/or slightly better than those reported by others for the weights of planktonic foraminifera (e.g., Marshall et al., 2013; Iwasaki et al., 2019a). This means that weights can be obtained with comparable accuracy without the use of an electronic microbalance. The stability of an electronic microbalance is generally affected by the surrounding environment, including environmental vibration, air temperature changes, electromagnetic interference, and static electricity, which tend to increase the measurement error. In the present study, we used an electronic ultra-microbalance, but the obtained variability was 8.2%, which was much greater than that obtained with μCT (1.3%). Our results suggest that our μCT approach is reliable and objective, and that it can be used for highly accurate analysis of the test bulk density of carbonate test.

The variation of the thresholds determined by the upper limit of air was relatively larger throughout the 2-month analysis period (STD = 7.2%). The cause of this variation is not well understood at this time but it may be related to day or long-term fluctuations in tube current or voltage, or changes in noise. The variation may affect not only the threshold for segmentation but also the *k* value, which is the relative position of the air and the peak value of the standard material (limestone). Further investigation is needed to determine the cause.

5.3 Aspects related to micropaleontology and paleoceanography

The weight of foraminifera and other marine calcifiers is a fundamental indicator of marine carbonate production through the Earth history. Therefore, obtaining accurate test bulk densities of marine calcifiers is extremely important from micropaleontology and paleoceanography perspectives. Furthermore, calculation of weight is important because it can be converted to carbon mass. Weak dissolution of foraminiferal tests in shallow water and at the sediment/water interface has been reported in only a few papers (e.g., Archer and Maier-Reimer, 1994; Schiebel et al., 2007). Although earlier studies have reconstructed carbonate ion concentrations from test fragmentation rates and weight changes of foraminifera (e.g., Broecker and Clark, 2001; de Villiers, 2005), direct measurement of test bulk density measurements are expected to further improve the accuracy of this method.

Traditionally, it has been extremely difficult to obtain information for the quantification of carbonate dissolution and reconstruction of [CO_3^{2-}] from poorly preserved deep-sea samples because of high fragmentation of the foraminiferal tests contained within the samples. Our μCT approach could potentially be applied to such fragmentated samples. In the past, attempts have been made to estimate the chemical properties of seawater, particularly its corrosiveness to calcium carbonate, from the extent of the fragmentation and morphological characteristics of the fragments of fossil tests (e.g., Adelseck, 1977; Ku and Oba, 1978). If the fragmentation is due to carbonate dissolution rather than physical destruction, then indications of the process of dissolution should remain in the fragments. If the fragmentation history can be identified through dissolution experiments in the laboratory, possible applications include elucidation of the intensity of carbonate dissolution and the resulting carbonate ion concentration by measuring the density of the fragments. As already mentioned, the major advantage of μCT analysis is that it is a nondestructive analysis, which allows geochemical analysis to be performed after morphometric measurements. After μCT measurements, stable isotope ratios and trace element analyses can be performed to reveal post-depositional alteration that occur with carbonate dissolution.

However, there are some points to note when using test bulk density as an index of carbonate dissolution. For example, when foraminiferal tests with two-layered structures are strongly affected by carbonate dissolution (Lohmann, 1995), the layer most vulnerable to carbonate dissolution is removed first, leaving behind the less-vulnerable layer (Berger, 1975; Johnstone et al., 2010; 2011; Iwasaki et al., 2015). A test that has undergone strong dissolution could still have a high CT number, which may lead to the erroneous conclusion that the individual test has not undergone dissolution. Therefore, when CT number is used as an index of the dissolution of marine calcifiers, it should be applied to species for which the dissolution process is known, and the CT numbers should always be considered together with the microstructure revealed by SEM, CT images, or both. This is also true when examining the thickness and volume of foraminiferal tests.

5.4 Aspects related to ocean acidification and modern oceanography

The progress of ocean acidification is an urgent global environmental issue. Quantifying test bulk density is extremely important for considering changes in the carbonate system under ocean acidification and its impacts on marine calcifiers. Many studies examining the changes in coastal water carbonate systems and their biological impacts have been conducted; however, few have been conducted on pelagic ecosystems. In particular, the relationships between ocean acidification and low-trophic level ecosystems are poorly understood. Orr et al. (2005) were the first to suggest the biological impacts of ocean acidification on shelled pteropods, and others have subsequently reported the impacts on thecosomatous pteropods, the tests of which contain aragonite, in the modern ocean (e.g., Doney et al., 2009; Bednaršek et al., 2014; Howes et al., 2017; Peck, et al., 2018; Bednaršek et al., 2021; Mekkes, et al., 2021; Niemi et al., 2021).

To understand the impact of ocean acidification on marine life, it is becoming increasingly important to undertake studies to observe test formation in marine organisms. For example, Wakita et al. (2013) have suggested that the total alkalinity of the western North Pacific in winter has remained unchanged in the last decade due to limited production

of calcium carbonate species. Calcification by marine calcifiers might also be suppressed in the northwestern North Pacific (e.g., Riebesell et al., 2000). Test bulk density measurements using μCT may help us to understand these phenomena. However, moving forward, long-term accumulation of data for the modern ocean will be needed, and for this an international framework that facilitates cooperation and expansion of analytical facilities will have to be established.

6 Conclusion

Here, we repeatedly measured the morphology (volume and CT number) of planktonic foraminifer by using μCT over a period of 2 months. Our findings demonstrate that μCT systems can be used to measure the test bulk density of calcareous tests and to examine their morphology with high accuracy.

In addition, the CT numbers of our novel artificial carbonate phantoms showed excellent linearity with independently measured bulk density, indicating their potential for use as reference materials to measure test bulk density of marine calcifiers. By calibrating CT numbers using these phantoms, we expect to be able to standardize measurement results between laboratories.

Data availability statement

The original contributions presented in the study are included in the article/Supplementary Material, further inquiries can be directed to the corresponding author.

Author contributions

KK and RH performed all experimental design and μCT analysis; OS and TI provided technical guidance and scientific advice on the CT analysis. All authors contributed to the article and approved the submitted version.

Funding

The author(s) declare financial support was received for the research, authorship, and/or publication of this article. This work was supported by JSPS KAKENHI grants (JP19H03037 and JP15H05712) and JAMSTEC operating grants.

Acknowledgments

Keisuke Shimizu contributed to the statistical evaluation and discussion of the data. Nina Bednaršek provided fruitful discussions regarding μCT analysis of marine calcifiers.

Conflict of interest

Author TI was employed by White Rabbit Corp.

The remaining authors declare that the research was conducted in the absence of any commercial or financial relationships that could be construed as a potential conflict of interest.

Publisher's note

References

Adelseck, J. C. G. (1977). Dissolution of deep-sea carbonate: preliminary calibration of preservational and morphologic aspects. *Deep-Sea Res.* 24 (12), 1167–1185. doi:10.1016/0146-6291(77)90520-3

Aldridge, D., Beer, C. J., and Purdie, D. A. (2012). Calcification in the planktonic foraminifera *Globigerina bulloides* linked to phosphate concentrations in surface waters of the North Atlantic Ocean. *Biogeosciences* 9, 1725–1739. doi:10.5194/bg-9-1725-2012

Archer, D., and Maier-Reimer, E. (1994). Effect of deep-sea sedimentary calcite preservation on atmospheric CO2 concentration. *Nature* 367, 260–263. doi:10.1038/367260a0

Arikawa, R. (1983). Distribution and taxonomy of globigerina pachyderma (ehrenberg) off the sanriku coast, northeast Japan. *Sci. Rep. Tohoku Univ. 2nd Ser. Geol.* 53, 103–157.

Ay, M. R., Mehranian, A., Maleki, A., Ghadiri, H., Ghafarian, P., and Zaidi, H. (2012). Experimental assessment of the influence of beam hardening filters on image quality and patient dose in volumetric 64-slice X-ray CT scanners. *Phys. Med.* 28, 249–260. doi:10.1016/j.ejmp.2012.03.005

Barker, S., and Elderfield, H. (2002). Foraminiferal calcification response to glacial-interglacial changes in atmospheric CO2. *Science* 297, 833–836. doi:10.1126/science.1072815

Bednaršek, N., Feely, R. A., Reum, J. C. P., Peterson, B., Menkel, J., Alin, S. R., et al. (2014). *Limacina helicina* shell dissolution as an indicator of declining habitat suitability owing to ocean acidification in the California Current Ecosystem. Proc. R. Soc. *B* 281, 20140123. doi:10.1098/rspb.2014.0123

Bednaršek, N., Naish, K.-A., Feely, R. A., Hauri, C., Kimoto, K., Hermann, A. J., et al. (2021). Integrated assessment of ocean acidification risks to pteropods in the northern high latitudes: regional comparison of exposure, sensitivity and adaptive capacity. *Front. Mar. Sci.* 8, 671497. doi:10.3389/fmars.2021.671497

Beer, C. J., Schiebel, R., and Wilson, P. A. (2010). Testing planktic foraminiferal shell weight as a surface water [CO_3^{2-}] proxy using plankton net samples. *Geology* 38, 103–106. doi:10.1130/G30150.1

Berger, W. H. (1975). "Dissolution of deep-sea carbonates: an introduction," in *Dissolution of deep-sea carbonates*. Editors W. V. Sliter, A. W. H. Bé, and W. H. Berger (Lawrence, KS, USA: Cushman Found. Foram. Res., Spec. Publ.), 13, 7–10.

Bijma, J., Hönisch, B., and Zeebe, R. E. (2002). Impact of the ocean carbonate chemistry on living foraminiferal shell weight: comment on "Carbonate ion concentration in glacial-age deep waters of the Caribbean Sea" by W. S. Broecker and E. Clark. *Geochem. Geophys. Geosyst.* 3, 1–7. doi:10.1029/2002GC000388

Briguglio, A., Woger, J., Wolfgring, E., and Hohenegger, J. (2014). "Changing investigation perspectives: methods and applications of computed tomography on larger benthic foraminifera," in *Approaches to study living foraminifera: collection, maintenance and experimentation*. Editors H. Kitazato and J. Bernhard (Springer), 55–70. doi:10.1007/978-4-431-54388-6_4

Broecker, W., and Clark, E. (2001). Reevaluation of the $CaCO_3$ size index paleocarbonate ion proxy. *Paleoceanogr* 16, 669–671. doi:10.1029/2001pa000660

Brummer, G.-J. A., Hemleben, C., and Spindler, M. (1987). Ontogeny of extant spinose planktonic foraminifera (Globigerinidae): a concept exemplified by *Globigerinoides sacculifer* (Brady) and *G. ruber* (d'Orbigny). *Mar. Micropaleontol.* 12, 357–381. doi:10.1016/0377-8398(87)90028-4

Charrieau, L. M., Nagai, Y., Kimoto, K., Dissard, D., Below, B., Fujita, K., et al. (2022). The coral reef-dwelling *Peneroplis* spp. shows calcification recovery to ocean acidification conditions. *Sci. Rep.* 12, 6373. doi:10.1038/s41598-022-10375-w

de Villiers, S. (2005). Foraminiferal shell-weight evidence for sedimentary calcite dissolution above the lysocline. *Deep Sea Res. Part I Ocean. Res. Pap.* 52 (5), 671–680. doi:10.1016/j.dsr.2004.11.014

Doney, S. C., Fabry, V., Feely, R. A., and Kleipas, J. A. (2009). Ocean acidification: the other CO2 problem. *Annu. Rev. Mar. Sci.* 1, 169–192. doi:10.1146/annurev.marine.010908.163834

Erez, J. (2003). The source of ions for biomineralization in foraminifera and their implications for paleoceanographic proxies. *Rev. Mineral. Geochem* 54 (1), 115–149. doi:10.2113/0540115

Fox, L., Stukins, S., Hill, T., and GilesMiller, C. (2020). Quantifying the effect of anthropogenic climate change on calcifying plankton. *Sci. Rep.* 10, 1620. doi:10.1038/s41598-020-58501-w

Haarmann, T., Hathorne, E. C., Mohtadi, M., Groeneveld, J., Kölling, M., and Bickert, T. (2011). Mg/Ca ratios of single planktonic foraminifer shells and the potential to reconstruct the thermal seasonality of the water column. *Paleoceanog* 26, PA3218. doi:10.1029/2010PA002091

Hounsfield, G. N. (1980). Computed medical imaging. *J. Comput. Assist. Tomogr.* 4, 665–674. doi:10.1097/00004728-198010000-00017

Howes, E. L., Eagle, R. A., Gattuso, J.-P., and Bijma, J. (2017). Comparison of mediterranean pteropod shell biometrics and ultrastructure from historical (1910 and 1921) and present day (2012) samples provides baseline for monitoring effects of global change. *PLoS ONE* 12, e0167891. doi:10.1371/journal.pone.0167891

Ikenoue, T., Bjørklund, K. R., Dumitrica, P., Krabberød, A. K., Kimoto, K., Matsuno, K., et al. (2016). Two new living Entactinaria (Radiolaria) species from the Arctic province: *Joergensenium arcticum* n. sp. and *Joergensenium clevei* n. sp. *Mar. Micropaleont* 124, 75–94. doi:10.1016/j.marmicro.2016.02.003

Iwasaki, S., Kimoto, K., Okazaki, Y., and Ikehara, M. (2019a). X-ray micro-CT scanning of tests of three planktic foraminiferal species to clarify dissolution process and progress. *Geochem Geophys* 20. doi:10.1029/2019GC008456

Iwasaki, S., Kimoto, K., Sasaki, O., Kano, H., Honda, M. C., and Okazaki, Y. (2015). Observation of the dissolution process of Globigerina bulloides tests (planktic foraminifera) by X-ray microcomputed tomography. *Paleoceanogr* 30, 317–331. doi:10.1002/2014PA002639

Iwasaki, S., Kimoto, K., Sasaki, O., Kano, H., and Uchida, H. (2019b). Sensitivity of planktic foraminiferal test bulk density to ocean acidification. *Sci. Rep.* 9, 9803. doi:10.1038/s41598-019-46041-x

Iwasaki, S., Lembke-Jene, L., Nagashima, K., Arz, H. W., Harada, N., Kimoto, K., et al. (2022). Evidence for late-glacial oceanic carbon redistribution and discharge from the Pacific Southern Ocean. *Nat. Comm.* 13, 6250. doi:10.1038/s41467-022-33753-4

Johnstone, H., Schulz, M., Barker, S., and Elderfield, H. (2010). Inside story: an X-ray computed tomography method for assessing dissolution in the tests of planktonic foraminifera. *Mar. Micropaleont* 77, 58–70. doi:10.1016/j.marmicro.2010.07.004

Johnstone, H., Yu, J., Elderfield, H., and Schulz, M. (2011). Improving temperature estimates derived from Mg/Ca of planktonic foraminifera using X-ray computed tomography–based dissolution index, XDX. *Paleoceanog* 26, PA1215. doi:10.1029/2009PA001902

Kachovich, S., Sheng, J., and Aitchison, J. C. (2019). Adding a new dimension to investigations of early radiolarian evolution. *Sci. Rep.* 9, 6450. doi:10.1038/s41598-019-42771-0

Kinoshita, S., Kuroyanagi, A., Kawahata, H., Fujita, K., Ishimura, T., Suzuki, A., et al. (2021). Temperature effects on the shell growth of a larger benthic foraminifer (*Sorites orbiculus*): results from culture experiments and micro X-ray computed tomography. *Mar. Micropaleont* 163, 101960. doi:10.1016/j.marmicro.2021.101960

Ku, T., and Oba, T. (1978). A method for quantitative evaluation of carbonate dissolution in deep-sea sediments and its application to paleoceanographic reconstruction. *Quat. Res.* 10 (1), 112–129. doi:10.1016/0033-5894(78)90016-9

Kuroyanagi, A., Irie, T., Kinoshita, S., Kawahata, H., Suzuki, A., Nishi, H., et al. (2021). Decrease in volume and density of foraminiferal shells with progressing ocean acidification. *Sci. Rep.* 11, 19988. doi:10.1038/s41598-021-99427-1

Lohmann, G. P. (1995). A model for variation in the chemistry of planktonic foraminifera due to secondary calcification and selective dissolution. *Paleoceanog* 10 (3), 445–457. doi:10.1029/95pa00059

Marshall, B. J., Thunell, R. C., Henehan, M., Astor, Y., and Wejnert, K. E. (2013). Planktonic foraminiferal area density as a proxy for carbonate ion concentration: a calibration study using the Cariaco Basin ocean time series. *Paleoceanogr* 28, 363–376. doi:10.1002/palo.20034

Mekkes, L., Renema, W., Bednaršek, N., Alin, S. R., Feely, R., Huisman, J., et al. (2021). Pteropods make thinner shells in the upwelling region of the California Current Ecosystem. *Sci. Rep.* 11, 1731. doi:10.1038/s41598-021-81131-9

Moy, A., Howard, W., Bray, S., and Trull, T. (2009). Reduced calcification in modern Southern Ocean planktonic foraminifera. *Nat. Geosci.* 2, 276–280. doi:10.1038/ngeo460

Naik, S. S., Godad, S. P., Naidu, P. D., and Ramaswamy, V. (2013). A comparison of *Globigerinoides ruber* calcification between upwelling and non-upwelling regions in the Arabian Sea. *J. Earth Syst. Sci.* 122, 1153–1159. doi:10.1007/s12040-013-0330-y

Niemi, A., Bednaršek, N., Michel, C., Feely, R. A., Williams, W., Azetsu-Scott, K., et al. (2021). Biological impact of ocean acidification in the Canadian arctic: widespread severe pteropod shell dissolution in amundsen gulf. *Front. Mar. Sci.* 8, 600184. doi:10.3389/fmars.2021.600184

Ofstad, S., Zamelczyk, K., Kimoto, K., Chierici, M., Fransson, A., and Rasmussen, T. L. (2021). Shell density of planktonic foraminifera and pteropod species *Limacina helicina* in the Barents Sea: relation to ontogeny and water chemistry. *PloS one* 16 (4), e0249178. doi:10.1371/journal.pone.0249178

Orr, J., Fabry, V., Aumont, O., Bopp, L., Doney, S., Feely, R. A., et al. (2005). Anthropogenic ocean acidification over the twenty-first century and its impact on calcifying organisms. *Nature* 437, 681–686. doi:10.1038/nature04095

Osborne, E. B., Thunell, R. C., Marshall, B. J., Holm, J. A., Tappa, E. J., Benitez-Nelson, C., et al. (2016). Calcification of the planktonic foraminifera *Globigerina bulloides* and carbonate ion concentration: results from the Santa Barbara Basin. *Paleoceanog Paleoclim* 31 (8), 1083–1102. doi:10.1002/2016PA002933

Otsu, N. (1980). Automatic threshold selection method based on discriminant and least squares criteria. *IEICE Trans.* J63-D (4), 349–356.

Peck, V. L., Oakes, R. L., Harper, E. M., Manno, C., and Tarling, G. A. (2018). Pteropods counter mechanical damage and dissolution through extensive shell repair. *Nat. Commun.* 9, 264. doi:10.1038/s41467-017-02692-w

Riebesell, U., Zondervan, I., Rost, B., Tortell, P. D., Zeebe, E. E., and Morel, F. M. M. (2000). Reduced calcification of marine plankton in response to increased atmospheric CO_2. *Nature* 407, 364–367. doi:10.1038/35030078

Schiebel, R., Barker, S., Lendt, R., Thomas, H., and Bollmann, J. (2007). Planktic foraminiferal dissolution in the twilight zone. *Deep-Sea Res. II* 54, 676–686. doi:10.1016/j.dsr2.2007.01.009

Schiebel, R., and Hemleben, C. (2017). Planktic foraminifers in the modern ocean. *Springer Berl. Heidelb.* doi:10.1007/978-3-662-50297-6

Shimizu, K., Kimoto, K., Noshita, K., Wakita, M., Fujiki, T., and Sasaki, T. (2017). Phylogeography of the pelagic snail *Limacina helicina* (gastropoda: thecosomata) in the subarctic western North Pacific. *J. Mollusc. Stud.* 84, 30–37. doi:10.1093/mollus/eyx040

Todd, C. L., Schmidt, D. N., Robinson, M. M., and De Schepper, S. (2020). Planktic foraminiferal test size and weight response to the late Pliocene environment. *Paleoceanog Paleoclim* 35, e2019PA003738. doi:10.1029/2019PA003738

Wakita, M., Watanabe, S., Honda, M., Nagano, A., Kimoto, K., Matsumoto, K., et al. (2013). Ocean acidification from 1997 to 2011 in the subarctic western North Pacific Ocean. *Biogeosciences* 10, 7817–7827. doi:10.5194/bg-10-7817-2013

Weinkauf, M. F. G., Zwick, M. M., and Kucera, M. (2020). Constraining the role of shell porosity in the regulation of shell calcification intensity in the modern planktonic foraminifer *Orbulina universa* d'Orbigny. *J. Foram Res.* 50 (2), 195–203. doi:10.2113/gsjfr.50.2.195

Xiao, Y., Suzuki, N., and He, W. (2017). Applications and limitations of Micro-XCT imaging in the studies of Permian radiolarians: a new genus with bi-polar main spines. *Acta Palaeontol. Pol.* 62 (3). doi:10.4202/app.00367.2017

Zarkogiannis, S., Fernandez, V., Greaves, M., Mortyn, P. G., Kontakiotis, G., and Antonarakou, A. (2020). X-ray tomographic data of planktonic foraminifera species *Globigerina bulloides* from the eastern tropical atlantic across termination II. *Gigabyte* 1, 1–10. doi:10.46471/gigabyte.5

Zarkogiannis, S. D., Iwasaki, S., Rae, J. W. B., Schmidt, M. W., Mortyn, P. G., Kontakiotis, G., et al. (2022). Calcification, dissolution and test properties of modern planktonic foraminifera from the central atlantic ocean. *Front. Mar. Sci.* 9, 864801. doi:10.3389/fmars.2022.864801